PAPER

Check for updates

Trinuclear rare earth pyridyl-β-diketonate complexes: developing new methods towards finding lost toroidal spin states†

Patrick Mangundu, [ID] [a] Kate E. Tanner,[a] Andrew Bloomfield, [ID] [b] Peter J. Barnard, [ID] [c] Keith F. White, [ID] [c] Curtis C. Ho, [ID] [a] Nageshwar R. Yepuri,[d] Richard A. Mole [ID] [e] and Rebecca O. Fuller [ID] *[a]

A series of rare earth (RE) 'triangles' have been synthesised to investigate the low energy excitations of toroic molecules using inelastic neutron scattering (INS) experiments. β-Diketonate, 1-(2-pyridinyl)-1,3-butandione (o-pbdH) has been employed to synthesise [{Ho$_3$(O)$_2$(o-pbd)$_3$Cl(H$_2$O)$_5$}$_2$]·8Cl·3H$_2$O·0.5EtOH (**1**) and [{Dy$_3$(O)$_2$(o-pbd)$_3$Cl(H$_2$O)$_5$}$_2$]·6Cl·2EtOH·2hexane (**2**). With further examples, [Ho$_3$(OH)$_2$(o-pbd)$_3$Cl(H$_2$O)$_3$(EtOH)$_2$]·3Cl (**3**), [{Ho$_3$(OH)$_2$(o-pbd)$_3$Cl(H$_2$O)$_5$}$_2$]·6Cl·2H$_2$O (**4**) and [Dy$_3$(O)(OH)(o-pbd)$_3$(NO$_3$)$_4$(H$_2$O)$_2$]·2NO$_3$·H$_2$O (**5**) aimed towards the generation of variation in coordinated ancillary ligands that are capable of reducing symmetry and inhibiting toroic behaviour. A sterically bulky 3-(1-naphthyl)-1-(2-pyridyl)-propane-1,3-dione (o-nppdH) ligand impeded the formation of the RE$_3$ motif with [Dy$_2$(O)$_2$(o-nppd)$_5$(H$_2$O)]·6Cl (**6**) isolated. The RE$_3$ complexes are structurally similar to known trinuclear based single molecular toroics (SMTs), including RE-β-diketonate analogues prone to mixing between electronic states. Consistent with these, a non-magnetic SMT ground state was not observable in the new complexes utilising conventional magnetometry. Spectroscopic confirmation of toroic properties with INS was attempted for the first time on **1** and the structurally similar SMT [Ho$_3$(OH)$_2$(o-dppd-d$_{10}$)$_3$Cl(H$_2$O)$_5$]. The observed intensity of a broad Lorentzian at 0.69(1) meV for [Ho$_3$(OH)$_2$(o-dppd)$_3$Cl(H$_2$O)$_5$] and 0.44(1) meV for **1**, is remarkably close to the calculated energy gap ~5 cm^{-1} (or 0.62 meV) and potentially provides a new probe that can validate complexes with a poorly separated toroidic ground state.

Introduction

Rare earth (RE) metal ions are normally trivalent, Lewis acids capable of coordinating to hard donor atoms, forming com-

[a]*School of Natural Sciences – Chemistry, University of Tasmania, Hobart, Tasmania, Australia. E-mail: rebecca.fuller@utas.edu.au*
[b]*School of Molecular and Life Sciences, Curtin University, Bentley, WA 6102, Australia*
[c]*Department of Biochemistry and Chemistry, La Trobe Institute for Molecular Science, La Trobe University, Victoria, Australia*
[d]*Australian Nuclear Science and Technology Organisation (ANSTO), National Deuteration Facility, New Illawarra Road, Lucas Heights, New South Wales, Australia*
[e]*Australian Nuclear Science and Technology Organisation (ANSTO), Australian Centre for Neutron Scattering, New Illawarra Road, Lucas Heights, New South Wales, Australia*

plexes suited to a variety of applications.[1] Careful design and control of the coordination reaction is essential to generate desirable properties, but is often complicated by the lability of the RE metal ions. While using high denticity ligands with RE metal ions is a common approach to overcome this, it is not suitable in all cases and often a more tailored approach is required. RE metal complexes being developed as single molecular toroids (SMT) are one example where the metal ions must adopt a particular symmetry to generates a noncollinear arrangement of spins capable of producing a toroidal magnetic moment (Fig. 1). In contrast to single molecular magnets, SMT molecules lack a magnetic moment and are incapable of interacting with an applied external magnetic field. Nonetheless they retain the capability of cooperation with charge and inversion. More than a fundamental curiosity, these properties make them ideal for magnetic data storage, multiferroics and quantum computing.[2,3]

To generate a toroic moment, it is critical that complexes have strong magnetic exchange between spins centres and
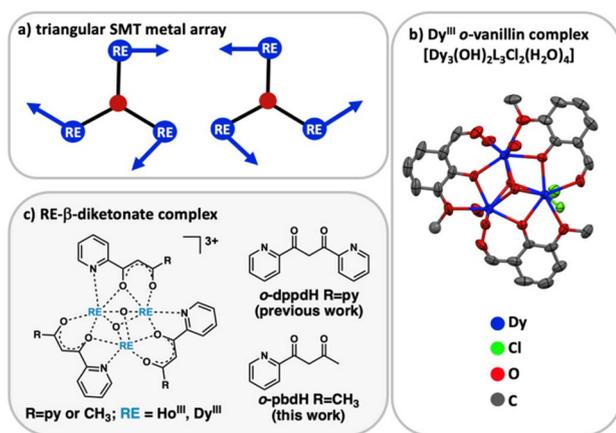
Fig. 1 (a) Schematic representation of triangular SMT metal array where the blue arrows are the local g_z magnetisation axes for the RE centre. (b) a structural representation of the $[Dy_3(OH)_2L_3Cl_2(H_2O)_4]$ complex with a triangular arrangement of Dy^{III} ions with the *o*-vanillin ligand (where L = 2-hydroxy-3-methoxy-benzaldehyde). (c) The general form of RE-β-diketonates "triangles" is $[RE_3(O(H))_2(L)_3Cl_x(H_2O)_y(EtOH)_z]$ where L = 1,3-bis(pyridin-2-yl)propane-1,3-dione (*o*-dppdH) or L = 1-(2-pyridinyl)-1,3-butandione (*o*-pbdH). Ancillary ligands are omitted for clarity.

appropriate symmetry constraints. There are a wide variety of architectures[4–6] and metal ions[7,8] capable of ensuring a suitable vortex spin arrangement.[9] The first reported SMT involved a triangular arrangement of Dy^{III} with *o*-vanillin ligands (Fig. 1b).[10] Each of the metal centres has a high symmetry triangular dodecahedron (TDD-8) environment, with a central μ-3 hydroxide above and below the metal coordination plane. The circular arrangement of spins is strongly anisotropic and aligns with the plane of the metal array. While the Cambridge Structural Database (CSD) contains ~250 reports of Dy complexes with a similar RE_3 coordination motif, only 31 of these are discrete homometallic structures and few (~20) reported to be SMTs (including linked $\{RE\}_n$ units).[2] Discrete homometallic holmium arrays of this form are even rarer, with only 4 entries contained in the CSD. Previous work to address this gap involved constructing RE metal 'triangles' using the highly versatile,[11] dipyridyl β-diketonate (Fig. 1c).[12] The similarity of the RE coordination environment[13] to the *o*-vanillin Dy^{III} system was expected to support an observable SMT behaviour. However, none of the pyridyl β-diketonate complexes exhibited the characteristic tailing in the magnetic isotherms. Though the result was not unexpected for the prolate Er^{III} complex, where significant transverse anisotropy will reduce axiality. For the oblate RE (Tb^{III}, Dy^{III}, Ho^{III}) complexes the unobserved toroidal moment was perturbed by high level calculations. These supported the ground state anisotropy of the Dy^{III} and Ho^{III} complexes having the required circular arrangement of spins and large ground state Ising anisotropy that is necessary for a toroidal spin arrangement. It seems likely that the small energy separation between the non-degenerate opposite spin ground states from the first excited state likely precluded SMT observation. Calculations for the Tb^{III} complex, revealed a

reduced axiality from different ancillary ligands and the resultant perpendicular value of the g tensor resulted in the complexes inability to support a toroidal moment. This work highlights a number of basic limitations when developing SMTs with a triangular RE motif: (i) complexes with small energy gap likely require an alternative experimental characterisation and (ii) even for a well-establish ligand families synthesising RE complexes with a predictable structure remains highly challenging. Addressing these concerns forms the basis of this work. With focus on developing a complementary characterisation using Inelastic Neutron Scattering (INS) experiments for a series of complexes with poorly separated ground states.

INS is a powerful technique for probing magnetic excitations across a wide range of materials.[14] The advantage of this method, is its ability to simultaneously observe excitations in both reciprocal space and energy, allowing one to determine spatial information about an excitation, in conjunction with its energy scale. This capability has been used extensively for 3d transition metal single molecule magnets (SMMs)[15] where the spin excitations are delocalised over several atoms. More recently, this has been extended to single crystals[16,17] which has allowed the 4D scattering function to be directly mapped and provide unprecedented insight into the spin correlation functions in molecular nanomagnets. The study of RE SMM's is comparatively limited and the bulk of these experiments have focused on single ion magnets,[18] where the energy scale is given by the crystal field splitting, which has a been a long-standing topic in condensed matter physics.[19] The key advance in recent years has been the integration of *ab initio* electronic structure calculations, which now allow detailed interpretation of crystal field excitations even in low symmetry molecular systems.[20] While a few studies have extended INS to multinuclear lanthanoid complexes, such as triangular clusters,[21] the application of this technique to more complex architectures remains limited. The current study expands the scope of INS by applying to a toroidal lanthanoid magnet.

Herein we report the detailed exploration of new SMT triangles with RE-β-diketonate complexes. With a number of well established approaches applied to β-diketonate coordination,[22] we have adopted careful ligand design to construct new family of complexes with the 1-(2-pyridinyl)-1,3-butandione (*o*-pbdH). The ligand has a structural similarity to previous triangles based on 1,3-bis(pyridin-2-yl)propane-1,3-dione (*o*-dppdH), a result not supported when using an alternate naphthyl functionalised β-diketonate. The synthesis of several *o*-pbdH RE_3 complexes with varied coordinated ancillary ligands has enabled an interrogation into whether the reduced axiality of the metal array can be controlled in these compounds. The new complexes generated further build our knowledge of the still infrequently reported SMTs, providing an unbiased viewpoint having not been previously synthesised. The generation of complexes predicted to have a small energy gap between the toroidal and first excited state provides an opportunity to address the limitations in characterisation of the SMT through INS experiments.

Results and discussion

Synthesis of complexes

β-Diketonates are known to resist ligand dissociation making this a sound choice the development of SMT systems.[23–25] Although examples using REs are part of an expansive field, the structural libraries are often produced *via* serendipitous discovery;[26] a consequence of both the versatile coordination behaviour of the β-diketonate and the propensity of RE to form various nuclearities (*i.e.* RE^{III} is labile in protic solvents).[27] To avoid this, and ensure the high symmetry environment required for an SMT, careful design is used to construct a new trinuclear clusters with the general form $[RE_3(O(H))_2(o\text{-pbd})_3Cl(H_2O)_x(EtOH)_y]\cdot S$ where $RE = Dy^{III}$ or Ho^{III}; $x + y = 5$; S = Cl, H_2O, CH_3CH_2OH (EtOH), hexane and/or pyridine (py) depending on work-up. The *o*-pbdH was synthesised *via* a Claisen condensation of ethyl-2-picolinate and acetone using a literature procedure (ESI Scheme S1†).[13,28] The ligand (2 equiv.) was treated with a RE salt (1 equiv.) of the form $RECl_3\cdot xH_2O$ ($RE = Ho^{III}$ or Dy^{III}). The method does not require the *in situ* generation of a base and works efficiently in conditions that are not strictly anhydrous. Both a 1 : 2 metal ion to ligand ratio and performing the reaction at elevated temperatures favours the formation of the trigonal products.[13] The crude product was purified using acetonitrile, pyridine then diethyl ether. The isolated complex underwent bulk recrystallised prior to INS and magnetometry experiments. Crystals suitable for X-ray diffraction were obtained by vapour diffusion, where a nonpolar solvent is slowly diffused into the solution[29] or slow evaporation. The solvent system used for work up is known to impact the solvent contained within the compound, to ensure the reproducibility of the coordinated co-ligand environment, preparation of the Ho^{III} complex was repeated twice and products crystallised thereof were found to be largely consistent with the form above. Structural modification was investigated *via* preparation of a further Dy₃ example from a $Dy(NO_3)_3\cdot xH_2O$ salt. The complex formed has a metal array consistent with the aforementioned RE₃ motif. The chloride and aqua ligands are replaced by four nitrates $[Dy_3(O)(OH)(o\text{-pbd})_3(NO_3)_4(H_2O)_2]$. The trinuclear array is not maintained when the bulky β-diketonate ligand 3-(1-naphthyl)-1-(2-pyridyl)-propane-1,3-dione (*o*-nppdH) is coordinated affording the dinuclear Dy complex $[Dy_2(o\text{-nppd})_5(H_2O)]$. This highlights the predisposition of β-diketonates to support a range of coordination environments and care must be taken to ensure the desired results in this case SMT 'triangles'.

Deuterated 1-(2-pyridinyl)-1,3-butanedione-d₉ (*o*-pbdH-d₉) and 1,3-di(pyridin-2-yl)propane-1,3-dione-d₁₀ (*o*-dppdH-d₁₀) ligands were synthesised (ESI Schemes S2 and S3†) to prepare complexes with reduced hydrogen content for INS measurements (H has a large incoherent scattering cross section). The deuterated precursors are generated from the hydrothermal metal-catalysed H/D exchange reaction of picolinic acid and 2-acetylpyridine in D_2O. Methyl ester of picolinate-d₄ was prepared in excellent yield by refluxing picolinic acid with methanol in the presence of a catalytic amount of H_2SO_4. The two deuterated 1,3-diketones prepared *via* Claisen condensation of

methyl picolinate-d₄ with either acetone-d₆ or acetylpyridine-d₇ in THF in presence of sodium hydride at 40 °C and 75 °C with yields around 63%. Finally, to obtain perdeuterated β-diketones an additional exchange with the keto–enol moiety was undertaken in CH_3OD at room temperature. The site-specific deuteration levels of the diketones measured by the integration of the ¹³C NMR spectrum[30] and using a reported formula. With an overall deuteration of 73% in *o*-pbdH-d₉ and 64% in *o*-dppdH-d₁₀ achieved.[30,31] The general experimental for complexation with these was analogous to methods used to prepare examples with the non-deuterated *o*-pbdH ligands. For this we chose to prepare holmium complexes, as compounds containing dysprosium are often complicated by strong neutron absorption. INS measurements require bulk crystalline material (~1 g). Attempts to directly scale-up complexation reactions introduced inconsistency in the composition of the prepared complexes. To prepare bulk powders three parallel small scale reactions were undertaken then combined during work up and bulk recrystallisation. The bridging methylene protons of the β-diketonates ligands are prone to substitution in protic solvents, consequently the final complexes used for INS likely have less than the 73%D and 64%D (Fig. S21 and S22†) in the as-synthesised ligand. To ensure the complexes are structurally consistent with the single crystals, $[Ho_3(O)_2(o\text{-pbd-d}_9)_3Cl(H_2O)_5]$ and $[Ho_3(OH)_2(o\text{-dppd-d}_{10})_3Cl(H_2O)_5]$ were characterised using pXRD and TGA analysis.

Crystallography

Fig. 2 contains a representation of the complex cation $[\{Ho_3(O)_2(o\text{-pbd})_3Cl(H_2O)_5\}_2]\cdot8Cl\cdot3H_2O\cdot0.5EtOH$ (**1**), a similar metal array (ESI Fig. S25–S34†) is observed in $[\{Dy_3(O)_2(o\text{-pbd})_3Cl(H_2O)_5\}_2]\cdot6Cl\cdot2EtOH\cdot2hexane$ (**2**), $[Ho_3(OH)_2(o\text{-pbd})_3Cl$
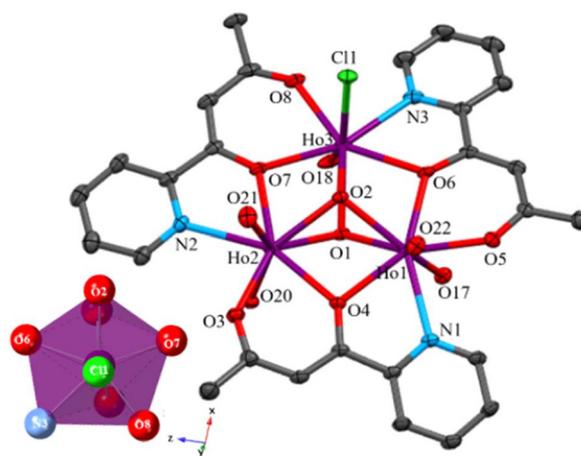
Fig. 2 Molecular structure of complex **1**. Ho⋯Ho distances are 3.52–3.56 Å. Thermal ellipsoids are set to 30% probability. For clarity, hydrogen atoms and lattice solvent are omitted. Inset contains the polyhedral view of the eight-coordinate geometry of Ho3 in complex **1**, the two μ₃-O are located above and below the RE centres. This depiction from CrystalMaker® v10.8.2 supports a TDD-8 coordination environment around the RE centre. Purple = Ho^{III}, red = O, green = Cl, grey = C and blue = N atom.

$(H_2O)_3(EtOH)_2]\cdot3Cl$ (**3**), $[\{Ho_3(OH)_2(o\text{-pbd})_3Cl(H_2O)_5\}_2]\cdot6Cl\cdot2H_2O$ (**4**) and $[Dy_3(O)(OH)(o\text{-pbd})_3(NO_3)_4(H_2O)_2]\cdot2NO_3\cdot H_2O$ (**5**). The compounds crystallise in the familiar trigonal motif, with two slightly different molecules observed in the unit cell of **1**, **2** and **4**. In each, the *o*-pbd ligands binds to two of the RE centres. One oxygen is shared (μ_2-O) and the other binds exclusively to one of the metal atoms. The RE–O–RE angle are slightly reduced when compared to the *o*-dppdH complexes, in **1** they range from 95.04–97.85° and in the second molecule 96.02–98.08°. Results are similar for **2–5** details are contained in the ESI (Table S7†). The nitrogen of the pyridyl ring is co-ordinated to the second metal centre so that each ligand is bound through $\mu\text{-}\eta^2(N,O);\eta^2(O,O')$ to the RE atom. The metal array is essentially a planar equilateral triangle with deviation from the ideal RE–RE–RE angle of less than 0.87°. Two central oxygen (or hydroxides) μ_3-O lie above and below ~1.2 Å the metal plane. One of the metal centres in each of **1–4** contains a single coordinated chloride ion. With the final positions in the eight coordinate cations containing H_2O and/or ethanol. Bond angle analysis reveals (ESI Tables S1, S3 and S4†) the terminal chloride ions for the Ho containing complexes results in the marginal change (~1°) of one RE–O–RE angle, which influences the magnetic exchange mechanism (ferromagnetism or antiferromagnetism) between the centres.

The calculated anisotropy axis in oblate RE_3 β-diketonate complexes is found to lie in the direction of the bridging keto oxo group. Co-ligands can modify this environment. Notably, the increased bond length ~2.7 Å of coordinating chloride ion when compared to coordinated oxygen atoms 2.3 Å (from water, methanol, or ethanol) is capable of reducing axiality when more than two metal centres contain terminal Cl bonds. The resulting reduction of the interaction between the ligand and oblate metal centre, means there is insufficient symmetry to support the circular toroidal spin arrangement. Consistency of one coordinated chloride ion per molecule in **1**, **3** and **4** eases any trepidation in complex reproducibility that may arise from RE lability. Further attempts to avoid the reduction symmetry from terminal chloride ions was attempted *via* use of a nitrate RE precursor for the synthesis of **5** (*cf.* use of $DyCl_3\cdot6H_2O$ in **2**). The metal array in $[Dy_3(O)(OH)(o\text{-pbd})_3(NO_3)_4(H_2O)_2]\cdot2NO_3\cdot H_2O$ is consistent with other RE-

β-diketonates 'triangles', with the nitro groups coordinating to the Dy^{III} centres *via* two different bonding modes. The Dy–O bond length of the nitrito (Dy–ONO$_2$) coordinated oxygen is similar/slightly longer in length (2.4 Å) to the coordinated aqua in **5** generating the required environment. The bidentate $\eta^2\text{-NO}_2$ coordination of three of the nitro ligands is noted to have two different bondlengths. One is comparable to the nitrito ~2.4 Å the other feature significantly elongated Dy–O lengths (~2.7 Å) close to Dy–Cl lengths. Numerous binding modes accessible by nitro co-ligands prevented the alleviation of symmetry concerns.

Using continuous shape measurements (Table 1) the 8-coordinate centre in **1** approximates a triangular dodecahedron (TDD-8) with D_{2d} symmetry (Fig. 2-inset). The RE metal centres are reminiscent of the environment in the *o*-vanillin complex (Fig. 1) and reported RE-β-diketonate SMTs based on *o*-dppdH ligand. Consequently, **1** is expected to have similar anisotropy and exchange interactions between the RE metal centres. Complexes **2**, **3** and **4** are observed in a similar TDD-8 arrangement (ESI Tables S2, S3 and S4 Fig. S26, S28, S30, S32†). Slight changes are noted in **5** which is calculated (ESI Table S5†) to be more consistent with a biaugmented trigonal prism (BTPR-8) with C_{2v} symmetry than the TDD-8 (for the later the refined distortion values indicate a reasonable approximation).

A further attempt to improve the axiality of these RE-β-diketonates complexes involved preparing a sterically bulky naphthyl bearing 3-(1-naphthyl)-1-(2-pyridyl)-propane-1,3-dione (*o*-nppdH) ligand. Complexation with Dy^{III} resulted in the formation of the dinuclear complex $[Dy_2(o\text{-nppd})_5(H_2O)]\cdot6Cl$ (**6**) (Fig. S35†) compound. Three ligands are bridged between the two Dy^{III} centres. One oxygen atom is shared (μ_2-O) and the other binds exclusively to one of the RE metal atoms. The nitrogen donor atom of the pyridine ring is also bonded. No chloride ions or solvent molecules are co-ordinated, instead these sites contain an additional *o*-nppd that is bound exclusively to a single Dy^{III} *via* the ligands' oxygen atoms. The metal centres are eight coordinate and approximate the BTPR-8 geometry with C_{2v} symmetry (ESI Table S6†), the TDD-8 is also reasonably approximated. The dinuclear array in **6**, is incapable of supporting the circular array of spins required for SMT behaviour.

Table 1 Selected interatomic distances and SHAPE parameter for $[\{Ho_3(O)_2(o\text{-pbd})_3Cl(H_2O)_5\}_2]\cdot8Cl\cdot3H_2O\cdot0.5EtOH$ (**1**) and $[\{Dy_3(O)_2(o\text{-pbd})_3Cl(H_2O)_5\}_2]\cdot6Cl\cdot2EtOH\cdot2hexane$ (**2**). Further lengths for these complexes and details for the other compounds are contained in the ESI

	1						**2**					
	Ho1	Ho2	Ho3	Ho4	Ho5	Ho6	Dy1	Dy2	Dy3	Dy4	Dy5	Dy6
Distances (Å)												
RE–Cl	—	2.660(1)	—	—	2.668(1)	—	2.668(3)	—	—	2.679(3)	—	—
RE–O1 (μ_3-O)	2.377(3)	2.383(3)	2.391(3)	2.366(3)	2.367(3)	2.389(3)	2.407(5)	2.365(6)	2.357(4)	2.398(6)	2.357(6)	2.354(8)
RE–O2 (μ_3-O)	2.336(3)	2.390(4)	2.350(3)	2.336(3)	2.402(3)	2.345(3)	2.379(6)	2.394(5)	2.388(6)	2.403(6)	2.378(7)	2.382(6)
RE–N	2.510(4)	2.511(4)	2.489(4)	2.504(4)	2.512(5)	2.497(5)	2.522(8)	2.504(9)	2.523(7)	2.55(3)	2.517(9)	2.521(8)
Distortion												
SHAPE (D_{2d})[a]	1.622	1.305	0.773	1.770	1.467	0.727	1.414	0.726	1.761	2.107	0.690	1.817

[a] D_{2d} symmetry for triangular dodecahedral polyhedral.

Magnetic properties

Measurements were made on polycrystalline samples of **1**, **2**, **5** and $[Ho_3(O)_2(o\text{-pbd-d}_9)_3Cl(H_2O)_5]$ restrained in Eicosane $(C_{20}H_{42})$ to prevent torquing. Results (Fig. 3-inset, ESI Fig. S37†) are similar to previous RE-β-diketonates complexes.[12] The room tempature $\chi_M T$ value for deuterated Ho^{III} complex is 42.80 cm^3 mol^{-1} K and the μ_{eff} per Ho^{III} 10.27μ_B. This is consistent with the calculated $g[J(J + 1)]^{0.5}$ values of 10.61μ_B per Ho^{III} centre. As temperature is decreased from room temperature a slight decrease in $\chi_M T$ product is observed and likely arisen from the progressive depopulation of the excited Stark levels. Below 20 K, there is a more rapid decrease in $\chi_M T$, that is probably associated with thermal depopulation of the low-lying Zeeman levels possibly combine with weak antiferromagnetic coupling between the Ho^{III} centres. Dy^{III} containing complexes **2** and **5** had room temperature $\chi_M T$ value of 40.43 and 39.05 cm^3 mol^{-1} K with μ_{eff} per Dy^{III} 10.38 and 10.22μ_B, respectively. These values are slightly lower than the calculated value of 10.65μ_B per Dy^{III} centre but consistent with a number of Dy$_3$ and toroic complexes.[32–34] Magnetisation (M) isotherms (2.5–7 K) were measured in DC fields of 0 to 7 T. The results for $[Ho_3(O)_2(o\text{-pbd-d}_9)_3Cl(H_2O)_5]$ are contained in Fig. 3. Similar results are observed for **1**, **2** and **5** (ESI Fig. S38†). In each, the measurements do not reach a saturation value at 7 T and at 2.5 K curve. The occurrence of low lying levels that are energetically close to the ground state support the role of zero field splitting or Zeeman depopulation effects evident by the non-superimposablility of the curves. In agreement with other trinuclear RE-β-diketonates,[12,13] the M vs. H curves at low fields do not have the S-shape tailing associated with toroidal systems, even though the metal ion coordination environments are comparable to reported examples.[10]
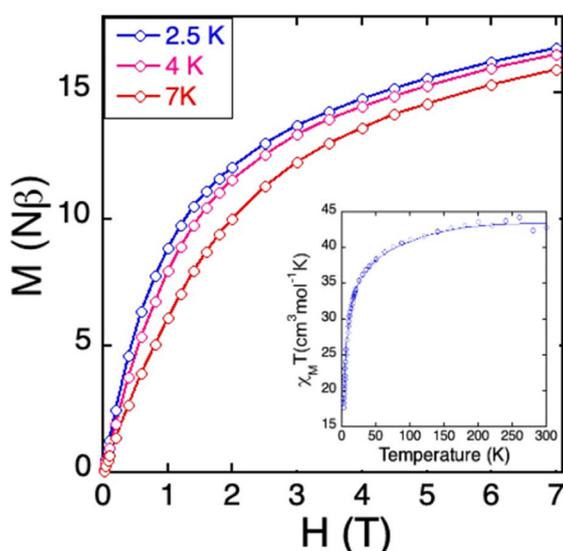
Variable temperature (2–7 K) AC dynamic measurements (180–1630 Hz) were undertaken without application of a DC bias field for complexes **1**, **2** and **5** (ESI Fig. S39–S40†). Expectedly, complexes **2** and **5** which contain Dy^{III} Kramers ions have an observable out of phase signal below 7 K that varies with frequency. No maxima are observed, as these multi-centred Dy^{III} complexes have insufficient anisotropy. In the absence of a bias field, holmium containing **1**, showed a limited response, the noisy data varied little with frequency.

Inelastic neutron scattering

The inability to observe a flattening in magnetic isotherms from the vortex arrangement of spins in RE-β-diketonates 'triangle' complexes, has been attributed to an energetically small separation of the non-magnetic ground state and first excited state. Experimental determination of magnetic anisotropy using polarized neutron diffraction[35] or understanding the role of pressure[36] are significant advancements for understanding these molecules and elucidating their relaxation processes. In order to determine the spectroscopic signature of a magneto-toroic complex we have performed inelastic neutron scattering on both the partially deuterated **1** and the previously reported $[Ho_3(OH)_2(o\text{-dppd-d}_{10})_3Cl(H_2O)_5]$ which has a validated toroidal state.[12] Unambiguously, the SINGLE_ANISO calculations at each Ho centre determined the metal array had a circular arrangement of ground state anisotropy that is capable of generating a toroid (ESI Fig. S43†). As the Ho$_3$ 'triangle' at the core of **1** and the deuterated version of the o-dppd complex are very similar we will use existing calculations to rationalise the data.

For both complexes we initially compare the Q integrated INS data, $S(\omega)$, at 1.5 K and 50 K (Fig. 4), these show very similar key features. Mainly a broad shoulder of intensity on
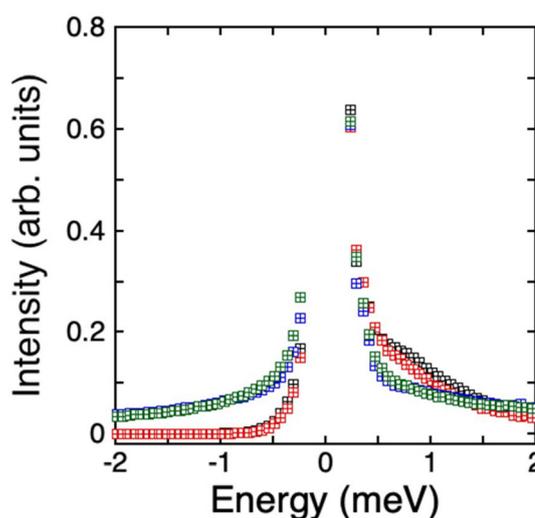

Fig. 3 The magnetic isotherms (2.5–7 K) in applied fields 0 to 7 T for the $[Ho_3(OH)_2(o\text{-pbd-d}_9)_3Cl(H_2O)_5]$. Inset contains the temperature dependent $\chi_M T$ in a DC field of 0.1 T.

Fig. 4 Plots of $S(\omega)$, **1** and $[Ho_3(OH)_2(o\text{-dppd-d}_{10})_3Cl(H_2O)_5]$. Where black is **1** at 1.5 K, red is $[Ho_3(OH)_2(o\text{-dppd-d}_{10})_3Cl(H_2O)_5]$ at 1.5 K, blue is **1** at 50 K and green is $[Ho_3(OH)_2(o\text{-dppd-d}_{10})_3Cl(H_2O)_5]$ at 50 K. Intensity is scaled to elastic line.

the elastic line at 1.5 K, while at 50 K, there is a broad quasi elastic response. To determine the origin of these effects, a constant energy cut was taken from each dataset at $E = 0.7(3)$ meV (ESI Fig. S41†). The results for this cut were almost identical for both samples, at 1.5 K there is a broad maximum at around 1 $Å^{-1}$ before reducing in energy. While at 50 K, the intensity increases with increasing Q. These cuts are consistent with the high temperature data being dominated by a QENS signal, while the low temperature shoulder on the elastic line is likely a magnetic signal. The temperature dependence of $S(\omega)$ for deuterated **1** and $[Ho_3(OH)_2(o\text{-dppd-d}_{10})_3Cl(H_2O)_5]$ (ESI Fig. S42†) shows that the QENS component is approximately independent of temperature, while the low energy shoulder increases with decreasing temperature. A low energy component like this, which is dependent on a low energy vibration or local diffusion process (e.g. water or methyl group rotation) is not unexpected, given the partially deuterated nature of the sample.

To confirm that the shoulder on the elastic line observed at low temperatures is magnetic the difference between the 1.5 K and 50 K cut was taken, which removes the temperature independent QENS contribution (Fig. 5). Again, the difference plot for both samples are very similar, with both showing a broad maximum at approx. 0.85 $Å^{-1}$ followed by a decrease in intensity for both samples. Such a reduction in intensity is indicative of the magnetic origin of this signal, this is because a magnetic signal is proportional to the magnetic form factor, which is determined by the Fourier transform of the unpaired electron density.[37] For an isolated rare earth ion, this can be approximated within the dipole approximation and appropriate values have been tabulated. The form factor of Ho^{III} is overlaid on Fig. 5 (blue dashed line). The form factor alone fails to

replicate the data, with the reduction in intensity of the data being far greater than that of the form-factor. As this is a Fourier transform, this implies that the electron density is over a larger volume than the free ion alone, this is typical of magnetic ions that interact with each other within a molecular cluster. The theory to understand this is well developed[38] and results in the magnetic signal being proportional to the product of the magnetic form factor and an interference term. For an equilateral trimer, the interference term is given by:

$$I(Q) \propto F^2(Q)\left(1 - \frac{\sin(QR)}{QR}\right) \quad (1)$$

where R is the interatomic distance for the magnetic ions, the solid blue line in Fig. 5, corresponds to the interference term with $R = 3.55$ Å, this is the average value of the Ho–Ho distances in both complexes. The fall-off in intensity at high Q is reasonably well replicated, but the position of the maximum is not. This difference between model and data is likely due to the fact we are using the subtraction between high and low temperature. However, the presence of maxima and the faster fall-off is indicative that this intensity cannot be ascribed to a single ion effect and is instead due to interactions within the Ho_3 clusters.

To determine the energy of this excitation and noting the contamination of the low energy QENS/vibration, we took a constant Q energy cut at $Q = 0.7(3)$ $Å^{-1}$ for both samples. These data were then fitted in the following manner.[39,40] A δ function was used to describe the elastic line while the inelastic feature was ascribed to either one or two Lorentzian functions as required, all of these functions were then convoluted with the experimental resolution function which was determined by measuring a vanadium standard and the constraint due to detailed balance (eqn (2)) was applied:

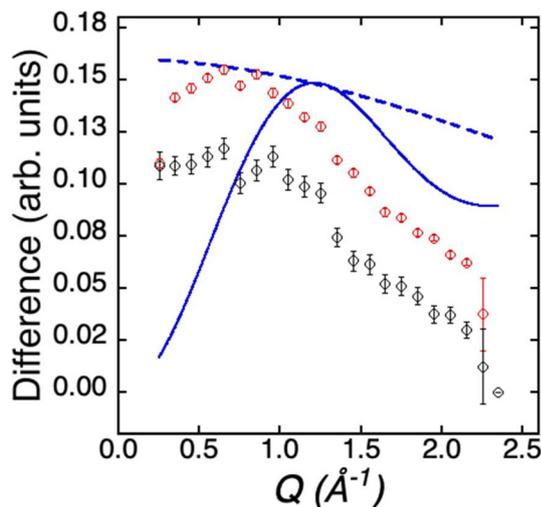$$S(Q, -\omega) = S(Q, \omega)e^{\frac{-\hbar\omega}{kT}} \quad (2)$$

The result of these fits is that for $[Ho_3(OH)_2(o\text{-dppd-d}_{10})_3Cl(H_2O)_5]$ we determined two Lorentzian contributions with centre 0.18(1) meV, FWHM 0.33(1) and centre 0.69(1) meV FWHM 0.57(2) meV. While for $[Ho_3(O)_2(o\text{-pbd-d}_9)Cl_5(H_2O)]$ centre 0.44(1) meV FWHM 0.55(1) meV (Fig. 6). Although deuterated **1** only shows one broad Lorentzian, the biggest deviation from the fit is in the low energy region closest to the elastic line.

These demonstrate that the magnetic excitations in both compounds are characterised by a broad low energy feature. This could either be ascribed to multiple low energy features, or the Lorentzian broadened feature could be indicative of very short-lived excitations. Although slight differences are noted, the similarity between spectra provides a first attempt to validate these observations and for the first time describe a spectroscopic signature of molecular toroidic behaviour. Specifically, the low energy inelastic neutron scattering spectrum it interpreted through the CASSCF Ab initio calculations performed using MOLCAS 8.0. The rare earth trimer is too large for efficient calculations to be carried out, so instead the

Fig. 5 Difference cuts of 1.5 K subtracted from 50 K constant energy Q slices at $E = 0.7(3)$ meV. The red circles are for $[Ho_3(OH)_2(o\text{-dppd-d}_{10})_3Cl(H_2O)_5]$ while the black circles are **1**. The dashed blue line is free ion form factor for Ho^{3+}, while the solid blue line is that described by eqn (1).
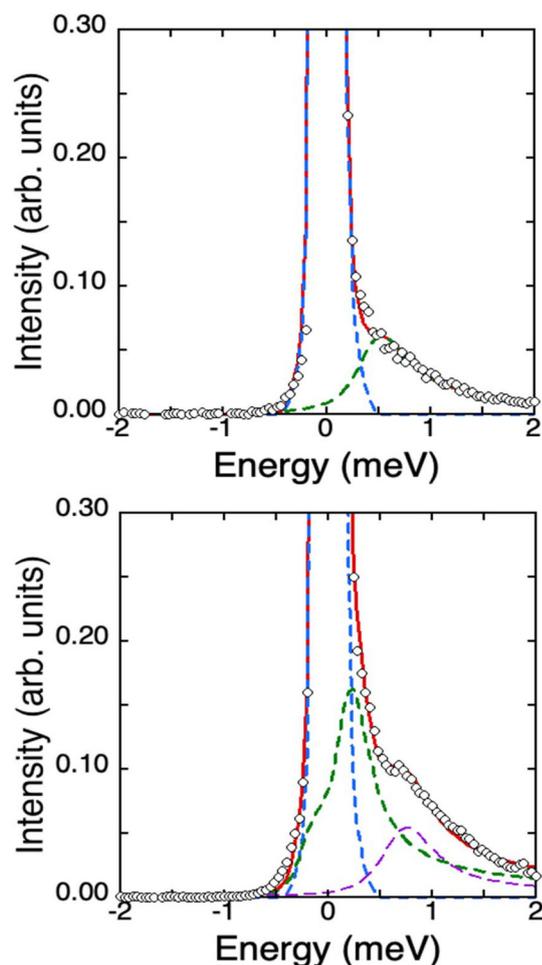
Fig. 6 Constant Q energy cuts at $Q = 0.7(3)$ Å^{-1} for [Ho$_3$(O)$_2$(o-pbd-d$_9$)Cl(H$_2$O)$_5$] (upper) and [Ho$_3$(OH)$_2$(o-dppd-d$_{10}$)$_3$Cl(H$_2$O)$_5$] (lower).

SINGLE_ANISO calculations were performed on trimers with two diamagnetic substitutions and then the exchange interactions were determine using the POLY_ANISO method. From these the low lying energy spectrum for the [Ho$_3$(OH)$_2$(o-dppd)$_3$Cl(H$_2$O)$_5$] complex is calculated to have an energy gap ~5 cm^{-1} between the first excited and ground state this is equivalent to 0.62 meV which is remarkably close to the observed intensity of the broad Lorentzian at 0.69(1) meV for [Ho$_3$(OH)$_2$(o-dppd-d$_{10}$)$_3$Cl(H$_2$O)$_5$] and 0.44(1) meV for deuterated **1** (ESI Fig. S43†).

A range of relaxation processes are possible for these molecules.[12] These include, a thermally assisted quantum tunnelling of magnetisation (TA-QTM), QTM and an Orbach relaxation. The complexity of the data means none of these pathways can be readily extracted. However, the presence of a broad Lorentzian component is consistent with very short lifetimes[18] even at low temperatures. Furthermore, the occurrence of low energy vibrational modes would be indicative of an allowed pathway for vibrational relaxation. However, to distinguish between the three proposed relaxation pathways would require

a combination of higher energy resolution measurements at dilution temperatures.

Conclusions

Reports of triangular RE$_3$ spin arrays with a nonmagnetic toroidal ground states are conspicuously absent, despite these compounds being well represented in the CSD. The inability to generate a coordination environment with sufficient ground state anisotropy to generate the vortex arrangement of spins that is energetically well separated from the first excited state is challenging. In this work we have developed a series of new RE-β-diketonate complexes with the express purpose to further elucidate methods to understand weakly coupled systems. Specifically, complexes containing a metal array of the general form [RE$_3$(O)$_2$(o-pbd)$_3$Cl(H$_2$O)$_x$L$_y$] where RE = Ho^{III} or Dy^{III} were synthesised. As with other RE-β-diketonate 'triangles', a flattening in the magnetic isotherms used to support a nonmagnetic ground state is not observed although the coordination environment mimics compounds with an observable toroidal moment. To date, calculations have been used to support the occurrence of low energy excitations and a small energy gap precluding the observation of the vortex spin arrangement *via* magnetometry. To complement this, we have feasibly developed a spectral signature for the characterisation of these toroic molecules using inelastic neutron scattering experiments. We observed for both a known SMT [Ho$_3$(OH)$_2$(o-dppd-d$_{10}$)$_3$Cl(H$_2$O)$_5$] and structurally similar molecule from this work (deuterated complex **1**) to have low energy INS data that is dominated by a very broad component likely from multiple low energy features, or very short-lived excitations. The energy of this feature is consistent with that predicted by *ab initio* calculations and is a hallmark of toroidic behaviour in these molecules.

Experimental

General experimental

All reactions were carried out under aerobic conditions with magnetic stirring unless otherwise stated. Reaction temperatures refer to oil bath temperatures, unless otherwise stated. All reactions involving heating were placed into a room temperature oil bath. Reagents were purchased from Sigma-Aldrich, Merck, Combi-Blocks, AK Scientific, Oakwood, Strem or Alfa Aesar and used without further purification unless otherwise stated. THF and toluene were deaerated *via* a nitrogen sparge then dried using an Innovative Technology solvent purification system. Thin layer chromatography (TLC) was performed on Silicycle silica gel 60 F$_{254}$ precoated aluminium sheets. Visualisation of developed plates was achieved through the use of a 254 nm or 365 nm UV lamp. Flash column chromatography was performed using silica gel as supplied by Merk® (chromatic silica particle size: 40–63 μm) and the indicated eluent in accordance with standard techniques.[41]

For deuterated ligands all reactions were performed under an atmosphere of nitrogen unless otherwise specified. Chemicals and reagents of the highest grade were purchased from Sigma-Aldrich (Sydney, Australia) and were used without further purification. Solvents were purchased from Sigma-Aldrich and Merck. NMR solvents were purchased from Cambridge Isotope Laboratories Inc. (MA, USA) and Sigma-Aldrich and were used without further purification. D_2O (99.8%) was supplied by AECL, Canada. Anhydrous dichloromethane, tetrahydrofuran and diethyl ether were obtained from a LC Technology Solutions Inc. SP-1 Stand Alone Solvent Purification System. Analytical thin-layer chromatography (TLC) was performed using Merck aluminium backed silica gel 60 F_{254} (0.2 mm) plates, which were visualised with shortwave (254 nm) ultraviolet light. Flash column chromatography was performed using Buchi Pure flash chromatography system with disposable silica gel cartridges, with the eluent mixture reported as the volume : volume ratio.

Physical measurements

Nuclear magnetic resonance spectra were recorded using a Bruker Avance III NMR operating at 600 MHz (^{1}H), 150 MHz or (^{13}C). All NMR spectra were calibrated to residual solvent signals. Data are reported as follows: chemical shift (ppm), multiplicity (s = singlet, d = doublet, t = triplet, m = multiplet, bs = broad singlet, dd = doublet of doublets, td = triplet of doublets, ABq = AB quartet), coupling constants (Hz), integration and assignment. Melting point data was collected using a Digimelt MPA161 melting point apparatus. Infrared (IR) spectroscopy was performed on an attenuated total reflectance PerkinElmer Spectrum 100 FT-IR with a diamond stage. Absorption spectra were recorded at room temperature using an Agilent Cary 60 UV-Vis spectrophotometer. TGA were performed using a Netzsch STA 449F5 from 25 to 500 °C with a heating rate of 20 K min^{-1}. Powder X-ray diffraction (XRD) patterns were obtained using a benchtop Bruker D2 phaser diffractometer with a Co X-ray anode. Elemental analyses were carried out on bulk samples using a Thermo FlashSmart Elemental Analyser. Inductively coupled plasma atomic emission spectroscopy (Murdoch-Marine and Freshwater Research Laboratory) was used to evaluate the RE content of the complexes. The metal analysis for the RE gave results consistent with the proposed formulations after extensive drying.

For deuterated ligands: low resolution electrospray ionization mass spectra (ESI-MS) were recorded on a 4000 QTrap AB SCIEX Mass Spectrometer. The overall percent deuteration of the molecules was calculated by ER-MS (enhanced resolution – MS) using the isotope distribution analysis of the different isotopologues by analysing the area under each MS peak which corresponds to a defined number of deuterium atoms. The contribution of the carbon-13 (natural abundance) to the value of the area under each $X + 1$ MS signal is subtracted based on the relative amount found in the protonated version. In a typical analysis we measure the carbon-13 natural abundance contribution by running ER-MS of the protonated version (or estimate it by Chem Draw software) and use this value in our calculation using an in-house developed spread sheet which subtracts this contribution from each MS signal constituting the isotope distribution. High-Resolution mass spectrometry was performed using a Shimadzu 9050 Time-of-flight spectrometer hyphenated to a Shimadzu 40 series UHPLC system. Samples (0.5 µL) were injected directly to the ESI source in a mobile phase of 80 : 20 MeCN : H_2O with 0.1% acetic acid as an ionisation aid at a flow rate of 0.4 mL min^{-1}. M/Z profile data was exported and analysed using DGet! to obtain the overall deuteration levels and the distribution of isotopologues.[31] ^{1}H NMR (400 MHz), ^{13}C NMR (100.6 MHz) and ^{2}H NMR (61.4 MHz) spectra were recorded on a Bruker 400 MHz spectrometer at 298 K. Chemical shifts, in ppm, were referenced to the residual signal of the corresponding NMR solvent. Deuterium NMR was performed using the probe's lock channel for direct observation.

Inelastic neutron scattering was performed using the Pelican instrument[42,43] at the Australian Centre for Neutron Scattering. The sample was held in an annular aluminium can, with thickness 0.5 mm chosen to minimise multiple scattering. Data were collected with the instrument configured for λ = 4.69 Å with an energy resolution of 0.135 meV. Data were corrected for background by subtracting an empty can and normalised using a vanadium standard. All data processing was carried out using the Mantid software.[44] Data were collected at 1.5 K, 10 K, 20 K, 30 K and 50 K for both wavelengths. Magnetic studies were performed using a Quantum Design Physical Property Measurement system or Quantum Design MPMS3 7Tesla SQUID magnetometer.

General synthesis for *o*-pbdH and *o*-nppdH complexes

o-pbdH (0.228 g, 0.0014 mol) or *o*-nppdH (0.385 g, 0.0014 mol) was dissolved in dry methanol (40 mL) under an inert atmosphere and triethylamine (0.2 mL, 1.4 mmol) was added dropwise to deprotonate the diketone. $RECl_3 \cdot 6H_2O$ where RE = Dy or Ho, was prepared by the reaction of RE_2O_3 and hydrochloric acid in aqueous solution. $RECl_3 \cdot 6H_2O$ (0.0007 mol) or $Dy(NO_3)_3 \cdot 5H_2O$ (0.0006 mol) was added to the reaction mixture and was heated at reflux for 72 h to ensure complete reaction. Following, the solvent was evaporated under reduced pressure, and the resulting solid was re-dissolved in 40 mL of acetonitrile to remove excess ligand. The mixture was then centrifuged at 7500 rpm for 5 minutes, and the insoluble residue was collected. The residue was subsequently dissolved in 40 mL of pyridine, and a second centrifugation was performed to precipitate any unreacted RE salt. The supernatant was collected and evaporated under reduced pressure. The resulting solid was purified by washing with diethyl ether (3 × 20 mL) to ensure purification. The target complex was either directly collected as a crystalline powder or recrystallized from methanol, ethanol, ethanol : H_2O (1 : 10) or a methanol : hexane mixture for further characterisation.

[{Ho$_3$(O)$_2$(*o*-pbd)$_3$Cl(H$_2$O)$_5$}$_2$]·8Cl·3H$_2$O·0.5EtOH (1)
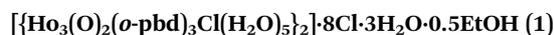
Yield: 0.66 g (63%). Crystals suitable for X-ray analysis were obtained by vapour diffusion of hexane into an ethanol solu-

tion after 6 weeks. MP: 210.3 °C. UV-vis (CH$_2$Cl$_2$): λ_{max}/nm (ε_{max} dm^3 mol^{-1} cm^{-1}): 327 (1.6 × 10^2) $\pi \rightarrow \pi^\star$. ATR-FTIR ($\nu$/cm^{-1}): 2923 w (C–H str.), 2853 w (C–H str.), 1405 s (C–O str.), 1310 m (C–N str.). Anal. calcd for [Ho$_3$(O)$_2$(o-pbd)$_3$Cl(EtOH) (H$_2$O)$_4$]·6Cl·6EtOH·5py = C$_{71}$H$_{99}$Cl$_7$Ho$_3$N$_8$O$_{19}$: C 40.39; H 4.73; N 5.31%. Found: C 40.60; H 4.70; N 5.04%. μ_{eff} = 10.40 B.M. per Ho^{3+}.

[{Dy$_3$(O)$_2$(o-pbd)$_3$Cl(H$_2$O)$_5$}$_2$]·6Cl·2EtOH·2hexane (2)

Yield: 0.64 g (61%). Crystals suitable for X-ray analysis were obtained by vapour diffusion of hexane into an ethanol solution after 6 weeks. MP: 206.0 °C. UV-vis (CH$_2$Cl$_2$): λ_{max}/nm (ε_{max} dm^3 mol^{-1} cm^{-1}): 325 (2.08 × 10^2) $\pi \rightarrow \pi^\star$. ATR-FTIR ($\nu$/cm^{-1}): 3174 w (C–H str.), 2953 w (C–H str.), 1405 s (C–O str.), 1310 m (C–N str.). Anal. calcd for [Dy$_3$(O)$_2$(o-pbd)$_3$Cl(H$_2$O)$_5$]·13Cl· 3EtOH·4py·8hex = C$_{101}$H$_{180}$Cl$_{14}$Dy$_3$N$_7$O$_{16}$: C 44.39; H 6.63; N 3.59%. Found: C 44.18; H 6.62; N 3.71%. %Dy calcd 17.8% found 17.1%. μ_{eff} = 10.38 B.M. per Dy^{3+}.

[Ho$_3$(OH)$_2$(o-pbd)$_3$Cl(H$_2$O)$_3$(EtOH)$_2$]·3Cl (3)

Yield: 0.18 g (43%). Crystals suitable for X-ray analysis were obtained by vapour diffusion of hexane into an ethanol solution after 4 weeks. MP: 208.3–211.1 °C. UV-vis (CH$_2$Cl$_2$): λ_{max}/nm (ε_{max} dm^3 mol^{-1} cm^{-1}): 334 $\pi \rightarrow \pi^\star$. ATR-FTIR ($\nu$/cm^{-1}): 3315 w (C–H *asym* stretch), 2973 w (C–H *sym* stretch), 1406 s (C–O stretch), 1360 m (C–N stretch). Anal. calcd for [Ho$_3$(OH)$_2$(o-pbd)$_3$Cl(H$_2$O)$_3$(EtOH)$_2$]·3.5Cl·4py = C$_{51}$H$_{60}$Cl$_{4.5}$Ho$_3$N$_7$O$_{13}$: C 37.50; H 3.70; N 6.00%. Found: C 37.74; H 3.45; N 6.19%.

[{Ho$_3$(OH)$_2$(o-pbd)$_3$Cl(H$_2$O)$_5$}$_2$]·6Cl·2H$_2$O (4)

Yield: 0.58 g (55%). Crystals suitable for X-ray analysis were obtained by vapour diffusion of hexane into an ethanol solution after 10 weeks. MP: 209 °C (dec). UV-vis (CH$_2$Cl$_2$): λ_{max}/nm (ε_{max} dm^3 mol^{-1} cm^{-1}): 327 (1.6 × 10^2) $\pi \rightarrow \pi^\star$. ATR-FTIR ($\nu$/cm^{-1}): 2921 w (C–H str.), 2848 w (C–H str.), 1410 s (C–O str.), 1310 m (C–N str.). Anal. calcd for [Ho$_3$(OH)$_2$(o-pbd)$_3$Cl (H$_2$O)$_5$]·3Cl·H$_2$O = C$_{27}$H$_{38}$Cl$_4$Ho$_3$N$_3$O$_{14}$: C 25.63; H 3.03; N 3.32%. Found: C 25.79; H 3.17; N 3.11%.

[Dy$_3$(O)(OH)(o-pbd)$_3$(NO$_3$)$_4$(H$_2$O)$_2$]·2NO$_3$·H$_2$O (5)

Yield: 0.42 g (24%). Crystals suitable for X-ray analysis were obtained by vapour diffusion of hexane into an ethanol solution after 4 weeks. MP: 192.6 °C. UV-vis (CH$_2$Cl$_2$): λ_{max}/nm (ε_{max} dm^3 mol^{-1} cm^{-1}): 361 (1.5 × 10^2) $\pi \rightarrow \pi^\star$. ATR-FTIR ($\nu$/cm^{-1}): 2922 w (C–H str.), 2834 w (C–H str.), 1434 s (C–O str.), 1320 m (C–N str.). Anal. calcd for [Dy$_3$(OH)O(o-pbd)$_3$(NO$_3$)$_3$]·8EtOH· py·8H$_2$O = C$_{48}$H$_{93}$Dy$_3$N$_7$O$_{33}$: C 32.32; H 5.25; N 5.50%. Found: C 32.64; H 5.18; N 5.72%. %Dy calcd 27.3% found 27.6%. μ_{eff} = 10.22 B.M. per Dy^{3+}.

[Dy$_2$(o-nppd)$_5$(H$_2$O)]·6Cl (6)

3-(1-Naphthyl)-1-(2-pyridyl)-propane-1,3-dione (0.39 g, 1.4 mmol), DyCl$_3$·6H$_2$O (0.26 g, 0.7 mmol) and triethylamine (0.2 mL, 1.4 mmol) were added to anhydrous MeOH (40 mL) and heated at reflux for 3 days. The mixture was concentrated

under reduced pressure and a 1 : 10 EtOH/H$_2$O v/v (55 mL) was added. The solution was filtered and concentrated under reduced pressure, yielding the crude product as a yellow solid (0.72 g, 68%). Crystals suitable for X-ray diffraction were obtained *via* vapour diffusion of hexane into an ethanol solution after 18 weeks. M.P. 248 °C. UV-vis (CH$_2$Cl$_2$): λ_{max}/nm (ε_{max} dm^3 mol^{-1} cm^{-1}): 375 (37 500) $\pi \rightarrow \pi^\star$. ATR-FTIR ($\nu$/cm^{-1}): 3370 w (O–H stretch), 2981 w (C–H *asym* stretch), 1447 s (C–O stretch), 1171 m (C–N stretch). Anal. calcd for [Dy$_2$(o-nppd)$_5$(H$_2$O)]·4Cl·2EtOH = C$_{94}$H$_{74}$Cl$_4$Dy$_2$N$_5$O$_{13}$: C 57.94; H 3.83; N 3.59%. Found: C 57.99; H 3.56; N 3.11%.

Synthesis of [Ho$_3$(O)$_2$(o-pbd-d$_9$)$_3$Cl(H$_2$O)$_5$] complex

Deuterated 1-(2-pyridinyl)-1,3-butanedione (o-pbdH-d$_9$) (0.23 g, 1.4 mmol) was added to anhydrous MeOH (~40 mL), followed by dropwise addition of triethylamine (0.20 mL, 1.4 mmol). HoCl$_3$·6H$_2$0 (0.266 g, 0.7 mmol) was added and the reaction heated at reflux for 24 h. The solvent was evaporated under reduced pressure and the solid was dissolved in 40 mL of acetonitrile (to remove excess ligand). This was centrifuged for 6 minutes at 2750 rpm. The insoluble solid was collected and dissolved in ~40 mL of pyridine, before being centrifuged again (unreacted RE salt precipitates out). The solution was collected and evaporated under reduced pressure and the yellow solid was then washed with diethyl ether (3 × 20 mL) and dried. Yield 0.16 g. MP: 219.4 °C. IR (ν/cm^{-1}): 2907 w (C–H str.), 1610 s (C–O str.), 1269 m (C–N str.) UV-vis (CH$_2$Cl$_2$): λ_{max}/nm (ε_{max} dm^3 mol^{-1} cm^{-1}): 325 (44 235) $\pi \rightarrow \pi^\star$. Anal. calcd for [Ho$_3(O)_2$($o$-pbd)$_3$Cl(H$_2$O)$_5$]·6Cl·5EtOH·6py = C$_{71}H_{88}Cl_7Ho_3N_8O_{17}$: C 40.95; N 6.05%. Found: C 40.73; N 6.21%. %Ho calcd 23.9% found 23.1%. μ_{eff} = 10.27 B.M. per Ho^{3+}. Powder X-ray analysis consistent with **1**.

Synthesis of [Ho$_3$(OH)$_2$(o-dppd-d$_{10}$)$_3$Cl(H$_2$O)$_5$] complex

Deuterated 1,3-di(2-pyridinyl)-1,3-propanedione (o-dppdH-d$_{10}$) (0.317 g, 1.4 mmol) was added to anhydrous MeOH (~40 mL), followed by dropwise addition of triethylamine (0.20 mL, 1.4 mmol). HoCl$_3$·6H$_2$0 (0.266 g, 0.7 mmol) was added and the reaction heated at reflux for 24 h. The solvent was evaporated under reduced pressure and the solid was dissolved in 40 mL of acetonitrile (to remove excess ligand). This was centrifuged for 6 minutes at 2750 rpm. The insoluble solid was collected and dissolved in ~40 mL of pyridine, before being centrifuged again (unreacted RE salt precipitates out). The solution was collected and evaporated under reduced pressure and the yellow solid was then washed with diethyl ether (3 × 20 mL) and dried. Yield 0.277 g. MP: 225.6 °C. IR (ν/cm^{-1}): 3179 w (OH str.), 3053 w (C–H str.), 2947 w (C–H str.), 1520 s (C–O str.), 1308 m (C–N str.). UV-vis (CH$_2$Cl$_2$): λ_{max}/nm (ε_{max} dm^3 mol^{-1} cm^{-1}): 316 (3.81 × 10^{-2}) $\pi \rightarrow \pi^\star$. Anal. calcd for [Ho$_3(OH)_2$($o$-dppd-d$_{10}$)$_3$Cl (H$_2$O)$_5$]·6Cl·6TEA·3EtOH = C$_{87}H_{156}Cl_8Ho_3N_{13}O_{16}$: C 43.32; N 7.54%. Found: C 43.20; N 7.52%. %Ho calcd 20.5% found 21.1%. Powder X-ray analysis consistent with the non-deuterated complex.[12]

Crystallography

Experimental data for the structures were measured at 150 K on a Rigaku Supernova diffractometer fitted with a Cu X-ray source and Hybrid Pixel Array Detector. In complexes **2**, **4** and **5** crystallographic disorder is apparent for some of the β-diketonate ligand atoms, where the data allowed, this disorder was modelled, and atoms assigned with anisotropic displacement parameters. For complex **5**, a Dy-coordinated nitrate group showed severe disorder, the disorder could not be modelled satisfactorily. Highly disordered non-coordinated solvent and counter ions were apparent for **1**, **2**, **4** and **6** for these atoms, the solvent mask procedure was used to remove reflections resulting from the electron density of the atoms from the HKL files. X-ray data collected on a crystal of complex **2**, revealed the crystal to be twinned; to process this data, a twin data reduction was employed. Crystallographic data for the structures reported in this paper have been deposited at the Cambridge Crystallographic Data Centre (CCDC 2448638–2448643†).

(**1**): $C_{64}H_{104}N_6O_{34}Ho_6Cl_{10}$ [{$Ho_3(O)_2(o\text{-pdb})_3Cl(H_2O)_5$}$_2$]·8Cl· $3H_2O$·0.5EtOH $M = 2845.61$, yellow irregular crystal, dimensions $0.18 \times 0.08 \times 0.03$ mm^3, monoclinic, space group $P2_1/n$, $a = 18.2181(2)$, $b = 15.5048(1)$, $c = 35.3931(4)$ Å, $\beta = 94.521(1)°$, $V = 9966.3(1)$ Å^3, $Z = 4$, $D_c = 1.8$ g cm^{-3}, $\mu = 11.551$ mm^{-1}. $F_{000} = 5496.0$, CuKα radiation, $\lambda = 1.54148$ Å, $2\theta_{max} = 7.496°$, 142,682, 144,140 reflections collected, 19,312 unique ($R_{int} = 0.0783$). Final GooF = 1.039, $R_1 = 0.0493$, w$R_2 = 0.1163$, R indices based on 19,312 reflections with $I > 2\sigma(I)$ (refinement on F^2), $|\Delta\rho|_{max} = 0.90$ e Å^{-3}, 975 parameters, 5 restraints. CCDC-2448642.†

(**2**): $C_{70}H_{107}N_6O_{28}Dy_6Cl_{10}$ [{$Dy_3(O)_2(o\text{-pdb})_3Cl(H_2O)_5$}$_2$]·6Cl· 2EtOH·2hexane $M = 2811.12$, colourless plate, $0.12 \times 0.08 \times 0.02$ mm^3, triclinic, space group $P\bar{1}$, $a = 15.6133(4)$, $b = 18.1248(6)$, $c = 18.1431(7)$ Å, $\alpha = 85.924(3)$, $\beta = 89.925(2)$, $\gamma = 74.263(3)°$, $V = 4928.5(3)$ Å^3, $Z = 2$, $D_c = 1.894$ g cm^{-3}, $\mu = 26.966$ mm^{-1}. $F_{000} = 2720$, CuKα radiation, $\lambda = 1.54184$ Å, $2\theta_{max} = 142.76°$, 52,996 reflections collected, 15,548 unique ($R_{int} = 0.0784$). Final GooF = 1.057, $R_1 = 0.0584$, w$R_2 = 0.1421$, R indices based on 15,548 reflections with $I > 2\sigma(I)$ (refinement on F^2), $|\Delta\rho|_{max} = 1.92$ e Å^{-3}, 924 parameters, 4 restraints CCDC 2448640.†

(**3**): $C_{31}H_{44}N_3O_{13}Ho_3Cl_4$ [$Ho_3(OH)_2(o\text{-pbd})_3Cl(H_2O)_3(EtOH)_2$]· 3Cl $M = 1301.27$, pink hexagons, $0.247 \times 0.148 \times 0.144$ mm^3, trigonal, space group $R\bar{3}$, $a = 31.8840(10)$, $b = 31.8840(10)$, $c = 26.8565(10)$ Å, $\alpha = 90$, $\beta = 90$, $\gamma = 120°$, $V = 23,644.24(17)$ Å^3, $Z = 18$, $D_c = 1.677$ g cm^{-3}, $\mu = 10.398$ mm^{-1}. $F_{000} = 11,466$, CuKα radiation, $\lambda = 1.54184$ Å, $2\theta_{max} = 151.51°$, 160,133 reflections collected, 10,844 unique ($R_{int} = 0.0490$). Final GooF = 1.043, $R1 = 0.0235$, w$R2 = 0.0615$, R indices based on 10,844 reflections with $I > 2\sigma(I)$ (refinement on F^2), $|\Delta\rho|_{max} = 0.61$ e Å^{-3}, 508 parameters, 24 restraints CCDC 2448643.†

(**4**): $C_{27}H_{40}N_3O_{15}Ho_3Cl_7$ [{$Ho_3(OH)_2(o\text{-pbd})_3Cl(H_2O)_5$}$_2$]·6Cl· 2H$_2$O $M = 1389.6$, pink plate, $0.23 \times 0.13 \times 0.05$ mm^3, triclinic, space group $P\bar{1}$, $a = 10.7890(2)$, $b = 13.8732(2)$, $c = 16.9814(4)$ Å, $\alpha = 106.212(2)$, $\beta = 100.122(2)$, $\gamma = 102.811(2)°$, $V = 2301.98(8)$ Å^3, $Z = 2$, $D_c = 2.005$ g cm^{-3}, $\mu = 13.494$ mm^{-1}. $F_{000} = 1326.0$, CuKα radiation, $\lambda = 1.54184$ Å, $2\theta_{max} = 142.548°$, 28,930 reflec-

tions collected, 8868 unique ($R_{int} = 0.0269$). Final GooF = 1.065, $R_1 = 0.0336$, w$R_2 = 0.0853$, R indices based on 8868 reflections with $I > 2\sigma(I)$ (refinement on F^2), $|\Delta\rho|_{max} = 1.70$ e Å^{-3}, 608 parameters, 2 restraints CCDC 2448638.†

(**5**): $C_{27}H_{31}N_9O_{29}Dy_3$ [$Dy_3(O)(OH)(o\text{-pbd})_3(NO_3)_4(H_2O)_2$]· 2NO$_3$·H$_2$O $M = 1433.11$, colourless plate, $0.07 \times 0.04 \times 0.02$ mm^3, monoclinic, space group $P2_1/c$, $a = 11.4903(3)$, $b = 19.5628(5)$, $c = 20.6987(5)$ Å, $\beta = 90.417(3)°$, $V = 4652.6(2)$ Å^3, $Z = 4$, $D_c = 2.046$ g cm^{-3}, $\mu = 26.301$ mm^{-1}. $F_{000} = 2744.0$, CuKα radiation, $\lambda = 1.54184$ Å, $2\theta_{max} = 143.728°$, 62,556 reflections collected, 8994 unique ($R_{int} = 0.1147$). Final GooF = 1.061, $R_1 = 0.0598$, w$R_2 = 0.1605$, R indices based on 8994 reflections with $I > 2\sigma(I)$ (refinement on F^2), $|\Delta\rho|_{max} = 1.31$ e Å^{-3}, 552 parameters, 1 restraints CCDC 2448641.†

(**6**): $C_{90}H_{62}N_5O_{11}Dy_2Cl_6$ [$Dy_2(o\text{-nppd})_5H_2O$]·6Cl $M = 1927.14$, colourless irregular crystal, $0.17 \times 0.07 \times 0.05$ mm^3, monoclinic, space group $P2_1/c$, $a = 9.9809(2)$, $b = 33.1510(5)$, $c = 26.2513(6)$ Å, $\beta = 100.700(3)°$, $V = 8534.9(3)$ Å^3, $Z = 4$, $D_c = 1.500$ g cm^{-3}, $\mu = 11.491$ mm^{-1}. $F_{000} = 3836.0$, CuKα radiation, $\lambda = 1.54184$ Å, $2\theta_{max} = 143.454°$, 37,130 reflections collected, 15,465 unique ($R_{int} = 0.0390$). Final GooF = 1.085, $R_1 = 0.0586$, w$R_2 = 0.1677$, R indices based on 15,465 reflections with $I > 2\sigma(I)$ (refinement on F^2), $|\Delta\rho|_{max} = 1.11$ e Å^{-3}, 1002 parameters, 6 restraints CCDC 2448639.†

Author contributions

P. M. synthesised compounds **1**, **2**, **4**, **5**, **6** and [$Ho_3(O)_2(o\text{-}$ pbd-d$_9$)$_3$Cl(H$_2$O)$_5$] in addition to characterisation of all compounds and undeuterated ligands. K. E. T. synthesised [$Ho_3(OH)_2(o\text{-dppd-d}_{10})_3Cl(H_2O)_5$] and A. B. synthesised **3**. P. J. B., K. F. W. and C. C. H. collected and analysed crystallographic data. N. R. Y. prepared o-dppdH-d$_{10}$ and o-pbd-d$_9$. R. A. M. performed and analysed INS. Along with R. O. F. conceptualised the project, measured and analysed magnetic data. R. O. F. prepared the manuscript with contributions from all authors.

Conflicts of interest

There are no conflicts to declare.

Data availability

The data supporting this article have been included as part of the ESI.† Crystallographic data for **1–6** has been deposited at the The Cambridge Crystallographic Data Centre (CCDC) under CCDC 2448638–2448643.†

Acknowledgements

References

1 S. P. Sinha, *Complexes of the rare earths*, Elsevier, 2013.

2 K. R. Vignesh and G. Rajaraman, *ACS Omega*, 2021, **6**, 32349–32364.

3 D. Plokhov, A. Pyatakov, A. Popov and A. K. Zvezdin, Spin-Electric Coupling, Magnetoelectricity, and Quantum Dynamics of Toroidal Moment in Lanthanide-Based Single Molecule Toroics, in *Single Molecule Toroics: Synthetic Strategies, Theory and Applications*, Springer, 2022, pp. 133–187.

4 P.-H. Guo, J.-L. Liu, Z.-M. Zhang, L. Ungur, L. F. Chibotaru, J.-D. Leng, F.-S. Guo and M.-L. Tong, *Inorg. Chem.*, 2012, **51**, 1233–1235.

5 S. K. Langley, B. Moubaraki, C. M. Forsyth, I. A. Gass and K. S. Murray, *Dalton Trans.*, 2010, **39**, 1705–1708.

6 S. Biswas, S. Das, T. Gupta, S. K. Singh, M. Pissas, G. Rajaraman and V. Chandrasekhar, *Chem. – Eur. J.*, 2016, **22**, 18532–18550.

7 S. K. Langley, K. R. Vignesh, B. Moubaraki, G. Rajaraman and K. S. Murray, *Chem. – Eur. J.*, 2019, **25**, 4156–4165.

8 J. Wu, L. Zhao, L. Zhang, X.-L. Li, M. Guo, A. K. Powell and J. Tang, *Angew. Chem., Int. Ed.*, 2016, **55**, 15574–15578.

9 K. Murray, *Single Molecule Toroics: Synthetic strategies, Theory and Applications*, Springer, Cham, 2022.

10 J. Tang, I. Hewitt, N. Madhu, G. Chastanet, W. Wernsdorfer, C. E. Anson, C. Benelli, R. Sessoli and A. K. Powell, *Angew. Chem., Int. Ed.*, 2006, **45**, 1729–1732.

11 G. Kurpik, W. Wachowicz, A. Walczak, J. Harrowfield and A. R. Stefankiewicz, *Coord. Chem. Rev.*, 2025, **539**, 216762.

12 C. Caporale, A. N. Sobolev, W. Phonsri, K. S. Murray, A. Swain, G. Rajaraman, M. I. Ogden, M. Massi and R. O. Fuller, *Dalton Trans.*, 2020, **49**, 17421–17432.

13 P. C. Andrews, G. B. Deacon, R. Frank, B. H. Fraser, P. C. Junk, J. G. MacLellan, M. Massi, B. Moubaraki, K. S. Murray and M. Silberstein, *Eur. J. Inorg. Chem.*, 2009, **2009**, 744–751.

14 B. T. M. Willis and C. J. Carlile, *Experimental Neutron Scattering*, Oxford University Press, 2008.

15 A. Furrer and O. Waldmann, *Rev. Mod. Phys.*, 2013, **85**, 367–420.

16 M. L. Baker, T. Guidi, S. Carretta, J. Ollivier, H. Mutka, H. U. Güdel, G. A. Timco, E. J. L. McInnes, G. Amoretti, R. E. P. Winpenny and P. Santini, *Nat. Phys.*, 2012, **8**, 906–911.

17 E. Garlatti, A. Chiesa, T. Guidi, G. Amoretti, P. Santini and S. Carretta, *Eur. J. Inorg. Chem.*, 2019, **2019**, 1106–1118.

18 M. A. Dunstan, R. A. Mole and C. Boskovic, *Eur. J. Inorg. Chem.*, 2019, **2019**, 1090–1105.

19 P. Fulde and M. Loewenhaupt, *Adv. Phys.*, 1985, **34**, 589–661.

20 M. Vonci, M. J. Giansiracusa, R. W. Gable, W. Van den Heuvel, K. Latham, B. Moubaraki, K. S. Murray, D. Yu, R. A. Mole, A. Soncini and C. Boskovic, *Chem. Commun.*, 2016, **52**, 2091–2094.

21 M. J. Giansiracusa, M. Vonci, W. Van den Heuvel, R. W. Gable, B. Moubaraki, K. S. Murray, D. Yu, R. A. Mole, A. Soncini and C. Boskovic, *Inorg. Chem.*, 2016, **55**, 5201–5214.

22 X. Yao, G. An, Y. Li, P. Yan, W. Li and G. Li, *J. Solid State Chem.*, 2019, **274**, 295–302.

23 K. Binnemans, *Handbook on the physics and chemistry of rare earths*, 2005, vol. 35, pp. 107–272.

24 A. Zaïm, N. Favera, L. Guénée, H. Nozary and T. Hoang, *Chem. Sci.*, 2013, **4**, 1125–1136.

25 E. S. Andreiadis, N. Gauthier, D. Imbert, R. Demadrille, J. Pecaut and M. Mazzanti, *Inorg. Chem.*, 2013, **52**, 14382–14390.

26 P. C. Andrews, W. J. Gee, P. C. Junk and M. Massi, *New J. Chem.*, 2013, **37**, 35–48.

27 K.-H. Yim, C.-T. Yeung, H.-Y. Wong and G.-L. Law, *Inorg. Chem. Front.*, 2021, **8**, 2952–2964.

28 V. Montoya, J. Pons, X. Solans, M. Font-Bardia and J. Ros, *Inorg. Chim. Acta*, 2005, **358**, 2763–2769.

29 S. V. Klementyeva, M. Y. Afonin, A. S. Bogomyakov, M. T. Gamer, P. W. Roesky and S. N. Konchenko, *Eur. J. Inorg. Chem.*, 2016, **2016**, 3666–3672.

30 T. A. Darwish, N. R. Yepuri, P. J. Holden and M. James, *Anal. Chim. Acta*, 2016, **927**, 89–98.

31 T. E. Lockwood and A. Angeloski, *J. Cheminf.*, 2024, **16**, 36.

32 T. Bereta, A. Mondal, K. Ślepokura, Y. Peng, A. K. Powell and J. Lisowski, *Inorg. Chem.*, 2019, **58**, 4201–4213.

33 X.-L. Li, H. Li, D.-M. Chen, C. Wang, J. Wu, J. Tang, W. Shi and P. Cheng, *Dalton Trans.*, 2015, **44**, 20316–20320.

34 C. Das, S. Vaidya, T. Gupta, J. M. Frost, M. Righi, E. K. Brechin, M. Affronte, G. Rajaraman and M. Shanmugam, *Chem. – Eur. J.*, 2015, **21**, 15639–15650.

35 E. A. Klahn, A. M. Thiel, R. B. Degn, I. Kibalin, A. Gukassov, C. Wilson, A. B. Canaj, M. Murrie and J. Overgaard, *Dalton Trans.*, 2021, **50**, 14207–14215.

36 V. S. Parmar, A. M. Thiel, M. S. Norre and J. Overgaard, *Cryst. Growth Des.*, 2023, **23**, 6410–6417.

37 S. W. Lovesey, *Theory of Neutron Scattering from Condensed Matter Volume II: Polarization Effects and Magnetic Scattering*, Oxford University press, 1986.

38 A. Furrer and H. U. Güdel, *Phys. Rev. Lett.*, 1977, **39**, 657–660.

39 A. M. Atkin, M. J. Giansiracusa, S. Calvello, E. Rousset, R. W. Gable, W. Phonsri, K. S. Murray, J. K. Howard, A. Soncini, R. A. Mole and C. Boskovic, *Inorg. Chem.*, 2023, **62**, 1141–1155.

40 M. A. Dunstan, M. J. Giansiracusa, M. Vonci, S. Calvello, D. Yu, A. Soncini, C. Boskovic and R. A. Mole, *Chem. Sci.*, 2023, **14**, 3990–4001.

41 W. C. Still, M. Kahn and A. Mitra, *J. Org. Chem.*, 1978, **43**, 2923–2925.

42 D. Yu, R. Mole, T. Noakes, S. Kennedy and R. Robinson, *J. Phys. Soc. Jpn.*, 2013, **82**, SA027.

43 D. Yu, R. A. Mole and G. J. Kearley, *EPJ Web Conf.*, 2015, **83**, DOI: **10.1051/epjconf/20158303019**.

44 O. Arnold, J. C. Bilheux, J. M. Borreguero, A. Buts, S. I. Campbell, L. Chapon, M. Doucet, N. Draper, R. Ferraz Leal, M. A. Gigg, V. E. Lynch, A. Markvardsen, D. J. Mikkelson, R. L. Mikkelson, R. Miller, K. Palmen, P. Parker, G. Passos, T. G. Perring, P. F. Peterson, S. Ren, M. A. Reuter, A. T. Savici, J. W. Taylor, R. J. Taylor, R. Tolchenov, W. Zhou and J. Zikovsky, *Nucl. Instrum. Methods Phys. Res., Sect. A*, 2014, **764**, 156–166.